Journal of Materials Chemistry B

ROYAL SOCIETY OF CHEMISTRY

PAPER



Cite this: *J. Mater. Chem. B*, 2024, **12**, 5838

# Comparative effectiveness of myocardial patches and intramyocardial injections in treating myocardial infarction with a MitoQ/hydrogel system

Ying Tan,†[a] Yali Nie,†[a] Lei ZhengWen†[b] and Zhi Zheng *[a]

In cardiac tissue engineering, myocardial surface patches and hydrogel intramyocardial injections represent the two primary hydrogel-based strategies for myocardial infarction (MI) treatment. However, the comparative effectiveness of these two treatments remains uncertain. Therefore, this study aimed to compare the effects of the two treatment modalities by designing a simple and reproducible hydrogel cross-linked with γ-PGA and 4-arm-PEG-SG. To improve mitochondrial damage in cardiomyocytes (CMs) during early MI, we incorporated the mitochondria-targeting antioxidant MitoQ into the hydrogel network. The hydrogel exhibited excellent biodegradability, biocompatibility, adhesion, and injectability *in vitro*. The hydrogel was utilized for rat MI treatment through both patch adhesion and intramyocardial injections. *In vivo* results demonstrated that the slow release of MitoQ peptide from the hydrogel hindered ROS production in CM, alleviated mitochondrial damage, and enhanced CM activity within 7 days, effectively inhibiting MI progression. Both hydrogel intramyocardial injections and patches exhibited positive therapeutic effects, with intramyocardial injections demonstrating superior efficacy in terms of cardiac function and structure in equivalent treatment cycles. In conclusion, we developed a MitoQ/hydrogel system that is easily prepared and can serve as both a myocardial patch and an intramyocardial injection for MI treatment, showing significant potential for clinical applications.

Received 19th March 2024,
Accepted 15th May 2024

DOI: 10.1039/d4tb00573b

rsc.li/materials-b

## 1. Introduction

Myocardial infarction (MI) ranks as a primary contributor to elevated mortality rates worldwide, representing a significant threat to public health.[1–3] Adult cardiomyocytes (CMs) exhibit a renewal rate of less than 1% per year and declines with age.[4,5] This phenomenon primarily arises from the highly polarized state of mature CMs, characterized by their prolonged residence in the G0 phase of the cell cycle, and the formation of an intricate network of tight junctions among CMs, collectively impeding the proliferation of adult CMs.[5,6] Moreover, insufficient oxygen supply, blood perfusion, and energy synthesis in the heart post-MI further diminish the proliferative capacity of CMs.[7,8]

Mitochondria are the most abundant organelles in CMs and play a crucial role in regulating cell proliferation, differentiation, and death.[9,10] After acute MI, ischemia and hypoxia result in mitochondrial dysfunction and the excessive generation of reactive oxygen species (ROS). Oxidative stress-induced damage by aberrant ROS is a significant contributor to cell cycle arrest and extensive cell death.[9,11] Studies have demonstrated that ROS generated from mitochondrial damage significantly impairs CM proliferation during the mouse embryonic stage, and the utilization of ROS inhibitors can effectively extend the therapeutic window for heart failure.[9,10] Sadek *et al.*[12] discovered that the proliferation period of CMs could be extended by mitigating mitochondria-dependent oxidative stress and DNA damage in CMs from mice and zebrafish. However, intravenous drug administration leads to a blind-end effect due to coronary artery obstruction, and the gene drug must attain a sufficient concentration at the target site to exert therapeutic effects. Current drug and surgical interventions focus on slowing disease progression rather than fully restoring cell proliferation and tissue regeneration in the infarcted area.

Tissue engineering and regenerative medicine represent highly desirable approaches for myocardial repair post-treatment of MI.[13] Hydrogels possess excellent mechanical properties and

[a] *Hunan Provincial Key Laboratory of Multi-omics And Artificial Intelligence of Cardiovascular Diseases &Department of Cardiology, The First Affiliated Hospital, Hunan Province Cooperative Innovation Center for Molecular Target New Drug Study & School of Pharmaceutical Science, Hengyang Medical School, University of South China, Hengyang, Hunan, 421001, China. E-mail: zhengzhi@usc.edu.cn*

[b] *Department of Cardiothoracic Surgery, The First Affiliated Hospital, Hengyang Medical School, University of South China, Hengyang, Hunan, 421001, China*

† These authors contributed equally to this work and should be considered co first authors.

biocompatibility, making them extensively studied in the field of tissue engineering.[14,15] The remarkable properties of hydrogels, such as the ability to create an extracellular matrix (ECM)-like microenvironment for damaged CMs and offer mechanical support to the impaired ventricular wall, have garnered significant attention in the treatment of MI.[14,16] In the field of cardiac tissue engineering, two primary treatment modalities are utilized: hydrogel patch adhesion onto the myocardial surface and hydrogel intramyocardial injection. Each treatment modality has distinct advantages and disadvantages. Injectable hydrogels enable direct delivery of the hydrogel into the inner myocardium, offering advantages such as *in situ* targeting, increased infarct wall thickness, and minimal invasiveness. However, they may also pose challenges, including fluid leakage, extended tissue damage, and inflammatory response.[14,17] In contrast, hydrogel patches reduce the risk of surgical invasiveness by utilizing polymeric materials capable of undergoing a sol–gel transition or incorporating memory-smart-responsive materials to load active substances into the hydrogel, thus promoting adhesion to and treatment of the infarcted area.[18,19] In comparison to hydrogel intramyocardial injections, the drug delivery of hydrogel patches necessitates traversing a dense myocardial layer, meeting increased wet adhesion requirements at the gel-solid interface, as well as possessing a higher level of surgical manipulation skills and experience.[18,20,21] Nevertheless, further clarification is required on the comparative effectiveness between the two therapeutic modalities: intramyocardial injections and hydrogel patches.

Therefore, the objective of this study was to compare the effectiveness of a hydrogel patch and hydrogel intramyocardial injection in treating MI, and to design a simple and easily reproducible injectable hydrogel with strong adhesion. The hydrogel was composed of γ-polyglutamic acid (γ-PGA) and 4-arm-PEG-SG, which exhibited excellent biodegradability, biocompatibility, adhesion, and injectability. We used this hydrogel to treat rats with MI by patch and intramyocardial injection, respectively. To improve the severe mitochondrial damage in early MI, the hydrogel network was loaded with the mitochondria-targeted antioxidant MitoQ. The MitoQ peptide was released gradually from the hydrogel, inhibiting ROS production in the CM, preventing oxidative damage in the mitochondria, and enhancing CM activity, thereby promoting myocardial repair. In conclusion, a simple and effective MitoQ/hydrogel system has been developed, showing significant potential for MI therapy as either a myocardial patch or intramyocardial injection.

**Zhi Zheng**

*Zhi Zheng is an Associate Professor at the Hengyang Medical School of University of South China. He received his PhD in Medicine under the supervision of Prof. Wei Hua and Prof. Cui-Yun Yu in 2022 from the University of South China. He set up his own research group in Wei Hua's team the University of South China since his PhD graduation. His research interests are in the study of cardiovascular disease pathogenesis and biomimetic microenvironmental delivery systems.*

## 2. Methods

### 2.1 Materials and reagents

γ-Polyglutamic acid (γ-PGA), *N*-hydroxysuccinimide (NHS), trimethylamine, 1-(3-dimethylaminopropyl)-3-ethylcarbodiimide hydrochloride (EDC·HCl), dopamine hydrochloride (DA), adipic dihydrazide, and $H_2O_2$ were provided by Aladdin (China). MitoQ (Mitoquinone) mesylate was purchased from Selleck (USA). 4-Arm-PEG-succinimidyl glutarate ester (4-arm-PEG-SG) was purchased from Xi'an KaiXin Biotechnology Co., Ltd. Anti-α-SMA, anti-Cx43, anti-vWF, anti-α-actinin, anti-CD31 affiniPure goat anti-mouse lg G (H+L), and affiniPure goat anti-rabbit lg G (H+L) were purchased from Proteintech (USA). Reactive oxygen species assay kit, Live/dead cell staining kit, and dihydroethidium assay kit were obtained from Beyotime (China). CMs (H9C2) was kindly provided by the Cell Bank of the Chinese Academy of Sciences. All other reagents and materials were of high quality unless otherwise stated.

### 2.2 Preparation of $NH_2$-γ-PGA-DA

1 g of γ-PGA was dissolved in distilled water and vigorously stirred. Then, 0.2 g of EDC and 0.12 g of NHS were added to the solution, and the pH was adjusted to 4.5 to activate the carboxyl groups for 4 hours. Afterwards, 0.3 g of dopamine hydrochloride was added to the mixture, and the reaction was allowed to proceed for 24 hours. After the reaction was completed, the mixture was dialyzed using an MD44 dialysis bag for a minimum of 3 days. Finally, the γ-PGA-DA product was frozen and then lyophilized to obtain the final product. For the $NH_2$-γ-PGA-DA synthesis, γ-PGA-DA was initially dissolved in distilled water and activated by adding 0.1 g of EDC and 0.06 g of NHS for 2 hours. Subsequently, oxalyl dihydrazide was added to the γ-PGA-DA solution and allowed to react for 24 hours. Finally, the reaction solution was dialyzed for 3 days and then lyophilized to obtain the $NH_2$-γ-PGA-DA product.

### 2.3 Preparation of MitoQ-loaded hydrogels

The hydrogel was formed through the amidation reaction between the amino groups on γ-PGA and the succinimide groups on 4-arm-PEG-SG. For the specific preparation of the hydrogel, such as the formulation of MitoQ (5 μM) loaded with 12.5 wt% $NH_2$-γ-PGA-DA and 12.5 wt% 4-arm PEG-SG, 25 mg of $NH_2$-γ-PGA-DA and 25 mg of 12.5 wt% 4-arm PEG-SG were dissolved separately in 200 mL of physiological PBS, and 5 μM of MitoQ was dissolved in one of the 200 mL PBS. The two solutions were then mixed and incubated at 37 °C until a MitoQ-loaded hydrogel was immediately formed.

### 2.4 Rheological testing of hydrogels

The rotational rheometer (Malvern, UK) was employed to analyze the storage modulus ($G'$) and loss modulus ($G''$) of cylindrical hydrogel specimens measuring 1 cm in diameter and 1 cm in height. Time sweep tests were carried out within the time frame of 0–20 minutes, while frequency sweep tests were performed within the frequency range of 0.1–10 Hz. These tests aimed to determine the final $G'$ and $G''$ values for each hydrogel sample. Additionally, stress–strain curves were generated by subjecting the cylindrical samples to compression at a rate of 0.5 mm $min^{-1}$ using an INSTRON 3365 universal material testing machine.

### 2.5 Degradation detection of hydrogels

In this study, we examined cylindrical hydrogel samples with dimensions of 1 cm in diameter and 1 cm in height. These samples were subjected to immersion in PBS at 37 °C. At regular intervals, the samples were taken out, freeze-dried, and weighed to determine the extent of degradation. The degradation cycle of the hydrogels was evaluated by calculating the ratio of mass lost to total mass.

### 2.6 Live/dead staining

Hydrogel precursor solution, measuring 10 μL per well, was used to inoculate CMs into 96-well plates. Following 12 hours of cell culture, the viability of the cells was evaluated using the CCK-8 assay. Additionally, the number of live and dead CMs was determined using Calcein-AM and PI staining, respectively, according to the kit's protocol (Solarbio, China). After incubation, the cells were rinsed with PBS, and the survival or proliferation of CMs was examined using a Nikon A1R laser confocal microscope. Calcein-AM staining resulted in a green fluorescence signal at 490 nm for live cells, while PI staining produced a red fluorescence signal at 545 nm for dead cells.

### 2.7 JC-1 staining

Cells from various sample treatments were collected from the culture solution and washed once with PBS. Following, 1 mL of JC-1 staining working solution was added and thoroughly mixed with the cells. The cells were then placed in a cell incubator at 37 °C for 20 minutes. After the incubation period, the supernatant was removed and the cells were washed twice with JC-1 staining buffer. Subsequently, 2 mL of cell culture solution was added and the cells were observed under a fluorescence microscope. The excitation light wavelength was set at 490 nm and the emission light wavelength was set at 530 nm.

### 2.8 Detection of ROS levels

The levels of intracellular superoxide anion and ROS were evaluated using dihydroethidium (DHE) and 2,7-dichlorodihydrofluorescein diacetate (DCFH-DA), respectively. CMs were cultured in 48-well plates with the addition of 0.1 mM $H_2O_2$ to induce cellular oxidative stress injury. Following this, the hydrogel precursor was applied to the CMs and incubated for 12 hours. DHE (5 mM) or DCFH-DA (10 μM) was used to stain the CMs. Nuclei were counterstained with DAPI and observed under a Nikon Ti A1 fluorescence microscope. The relative fluorescence intensity of DHE and DCFH-DA was quantified using ImageJ-Pro Plus 6.0. Moreover, infarct tissue samples were collected on days 3 and 5 post-treatment and treated with 5 mM DHE for 20 minutes. After washing with PBS, the sectioned samples were stained with DAPI and examined under a microscope. The DHE fluorescence intensity was measured in the infarct tissue samples on days 3 and 5. The infarct tissue was homogenized using a glass homogenizer in homogenization buffer, followed by centrifugation at 1000 rpm for 10 minutes at 4 °C to collect the supernatant. The supernatant was then mixed with the DHE solution and incubated for 30 minutes at 37 °C, as per the protocol. Fluorescence intensity was detected using a microplate reader with excitation at 535 nm and emission at 610 nm.

### 2.9 Detection of MitoQ release

The hydrogel loaded with FITC-MitoQ was immersed in PBS and gently agitated under conditions protecting it from light. Samples of 1 mL were collected at predetermined intervals, and an equal volume of fresh PBS was replenished. Subsequently, the absorbance of the solution, containing FITC-MitoQ, was determined at 490 nm using a UV-Vis spectrophotometer. The cumulative release profile of FITC-MitoQ from the hydrogels was calculated based on the standard calibration curve for FITC-MitoQ.

### 2.10 Establishment of MI rat model

A batch of 100 male SD rats (250 ± 30 g) was procured from Hunan Sja Laboratory Animal Co., Ltd (Changsha, China) for the study. To establish a MI model, the left anterior descending branch of the rat heart was ligated at the proximal end, following a previously documented procedure.[15,22] Subsequently, 100 μL of hydrogel was injected into five different regions of the infarcted area, with 20 μL being administered to each region. The hydrogel patch was directly applied to the surface of the infarcted myocardium within the pericardium, using 100 μL of hydrogel. During the construction of the MI model and subsequent survival phase, a total of 8 rats died. All experimental designs and protocols involving animals were approved by the Experimental Animal Ethics Committee of the University of South China, Hunan, People's Republic of China (approval 4304079008946) and complied with the National Institutes of Health and University of South China guidelines on the care and use of animals for scientific purposes.

### 2.11 Histological analysis

After euthanizing the rats, their hearts were excised and processed for further analysis. The hearts were fixed in a 4% paraformaldehyde solution, followed by paraffin embedding and sectioning. The fibrosis area was evaluated through H&E and Masson staining methods. Additionally, α-actinin staining was performed to visualize the cardiac cytoskeleton, while TUNEL staining was used to identify apoptotic cells. The nuclei

 

were counterstained with DAPI. Fluorescence microscopy was employed to observe and quantify the number of TUNEL-positive cells and normal cells in the infarcted tissue.

### 2.12 Echocardiographic analysis

Cardiac function assessment was performed on all rat groups at specific time points (days 7, 14, 21, and 28) post-surgery using a VisualSonics VEVO2100 small animal ultrasound system. Two-dimensional transthoracic echocardiography in M-mode was conducted under isoflurane anesthesia to evaluate cardiac function. Echocardiography measurements, including left ventricular ejection fraction (LVEF), left ventricular fractional shortening (LVFS), left ventricular internal diameter at end-diastole (LVIDD), and left ventricular internal diameter at end-systole (LVIDS), were obtained for all rats.

### 2.13 Immunofluorescence analysis

The infarcted areas of the heart samples were sectioned and subjected to a sequential incubation process involving specific primary and secondary antibodies. This was followed by DAPI staining to visualize the nuclei. The stained tissues were then examined under a fluorescence microscope. The vessel density in the infarcted heart tissues was assessed using primary antibodies against α-SMA and vWF. Additionally, the expression levels of proteins associated with systolic–diastolic coupling and myocardial electrical signaling, namely α-actinin and Cx43, respectively, were measured. The ImageJ was employed for the quantification and analysis of protein expression in each region of interest.

### 2.14 Statistical analysis

The results were presented as the mean ± standard deviation and subjected to one-way analysis of variance (ANOVA) to compare the means across multiple groups. Statistical significance was denoted as $^{*}P < 0.05$, $^{**}P < 0.01$, and $^{***}P < 0.001$.

## 3. Results and discussion

### 3.1 Preparation of $NH_2$-γ-PGA-DA/4-arm-PEG-SG hydrogels

To achieve both strong adhesion and injectability, we successfully prepared hydrogels utilizing a simple and reproducible strategy involving $NH_2$-γ-PGA-DA and 4-arm-PEG-SG (Fig. 1A). γ-PGA was extracted from natto and exhibited excellent water solubility, biodegradability, and adhesive properties far superior to those of hyaluronic acid.[23,24] To endow γ-PGA with cross-linking sites for hydrogel formation and adhesive tissue properties, we modified DA and adipic dihydrazide onto γ-PGA, respectively. The results showed that distinct characteristic peaks were observed at about 1.5 ppm and 6.6 ppm by $^1$H NMR spectroscopy, confirming the successful synthesis of $NH_2$-γ-PGA-DA through the presence of adipic dihydrazide and DA peaks. Integration of the peak area revealed a DA modification rate of approximately 15.5% and an amination level exceeding 80% (Fig. 1B). Likewise, the presence of characteristic peaks at 2.9 (a), 2.0 (b), and 3.4 (d) ppm in the $^1$H NMR spectra

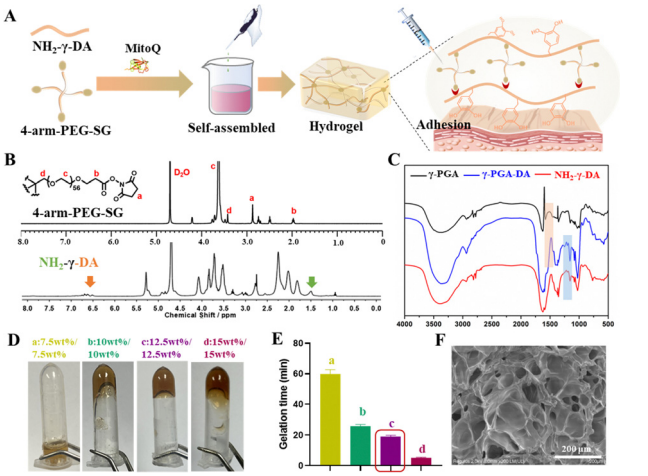


Fig. 1 Preparation of $NH_2$-γ-PGA-DA/4-arm-PEG-SG hydrogels. (A) Preparation procedure of $NH_2$-γ-PGA-DA/4-arm-PEG-SG hydrogels. (B) $^1$H NMR spectra of $NH_2$-γ-PGA-DA and 4-arm-PEG-SG. (C) FT-IR spectra of γ-PGA, γ-PGA-DA, and $NH_2$-γ-PGA-DA. (D) Photographs of gel time at different composition ratios. (E) Gel time of different proportions of hydrogels. (F) SEM image of $NH_2$-γ-PGA-DA/4-arm-PEG-SG hydrogels (scale bars: 200 μm).

confirmed the successful synthesis of 4-arm-PEG-SG (Fig. 1B). Additionally, the successful synthesis of $NH_2$-γ-PGA-DA was confirmed by FT-IR spectra, which exhibited amide I and II bands at 1528 $cm^{-1}$ and 1581 $cm^{-1}$, along with the stretching vibration of amide (C–N) observed at 1200–1350 $cm^{-1}$ (Fig. 1C).

Excessive gelation time can result in hydrogel loss within the myocardium, whereas insufficient gelation time may lead to needle blockage.[14] To optimize the gelation time of the hydrogel, we varied the ratio of components and employed the inversion method to monitor gelation time. Experimental results demonstrated that a mixture consisting of 12.5 wt% $NH_2$-γ-PGA-DA and 12.5 wt% 4-arm PEG-SG achieved gelation within approximately 19 minutes at 37 °C and pH 7.5 (Fig. 1D and E). Despite the shorter gelation time of 15 wt%/15 wt% $NH_2$-γ-PGA-DA/4-arm PEG-SG hydrogels, their higher mechanical strength renders them unsuitable for subsequent adhesion to the myocardial surface. Scanning electron microscopy (SEM) analysis revealed that the lyophilized hydrogels exhibited a uniform three-dimensional network structure, enabling efficient drug encapsulation, release, and cell migration (Fig. 1F).

### 3.2 Characterization of $NH_2$-γ-PGA-DA/4-arm-PEG-SG hydrogels

Hydrogels with appropriate mechanical strength can prevent collapse of the myocardial wall after MI by supporting the infarcted myocardial wall.[25,26] However, increased mechanical strength results in the formation of a highly dense gel network within the hydrogel, impeding drug release and hindering gel adhesion to the myocardial surface. Rheology is a commonly employed method for evaluating the mechanical properties of hydrogels. $G'$ and $G''$ of 12.5%/12.5% and 15%/15% hydrogels were measured using time-scan mode over a period of 20 minutes. The results indicated that the modulus of the 15%/15% hydrogels increased with an increase in the concentration of the unit

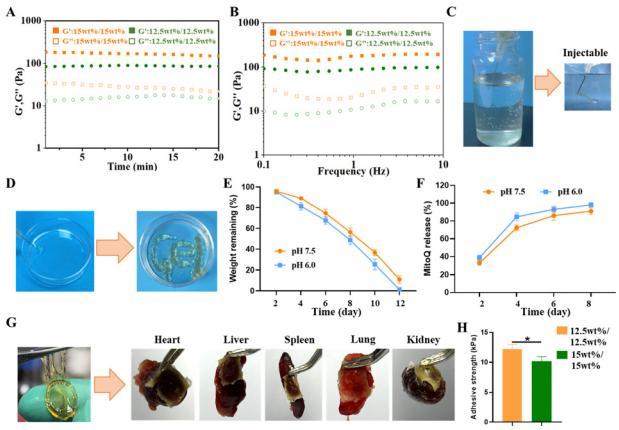


Fig. 2 Characterisation of $NH_2$-γ-PGA-DA/4-arm-PEG-SG hydrogels. (A) Rheological time scanning plots of $NH_2$-γ-PGA-DA/4-arm-PEG-SG hydrogels. (B) Rheological frequency scanning plots of $NH_2$-γ-PGA-DA/4-arm-PEG-SG hydrogels. (C) and (D) Photographs of the injectability of $NH_2$-γ-PGA-DA/4-arm-PEG-SG hydrogels. (E) Weight retention of the hydrogels at pH 7.5 and pH 6.0. (F) Drug release cycle of the hydrogels at pH 7.5 and pH 6.0. (G) Photograph of $NH_2$-γ-PGA-DA/4-arm-PEG-SG hydrogels adhering to the heart, liver, spleen, lungs, and kidneys. (H) Adhesion strength of $NH_2$-γ-PGA-DA/4-arm-PEG-SG hydrogels.

component (Fig. 2A). In the frequency scanning mode, $G'$ consistently exceeded $G''$ within the 0.1 to 10 Hz range, indicating the formation of a crosslinked network resembling an elastic solid in all hydrogel samples, with the 15%/15% hydrogels exhibiting greater mechanical strength (Fig. 2B). Both hydrogels were then tested for injectability using a 28-gauge insulin needle. The findings indicate that the hydrogels with a concentration of 12.5%/12.5% were easily extruded through the needle, whereas those with a concentration of 15%/15% encountered resistance (Fig. 2C and D).

During the early stage of MI, which typically lasts for about one week, a significant number of CMs undergo cell death. These deceased cells attract inflammatory factors that contribute to the accelerated progression of MI. The $NH_2$-γ-PGA-DA/4-arm-PEG-SG hydrogel demonstrates remarkable biodegradability. Cylindrical $NH_2$-γ-PGA-DA/4-arm-PEG-SG hydrogels, measuring 1 cm in both diameter and height, were immersed in pH 7.5 PBS, and the results showed that the hydrogel was completely degraded within 12 days. Moreover, the degradability and release profile of MitoQ in this hydrogel were assessed in a weakly acidic pH 6.0 environment. The hydrogel exhibited slightly faster degradation in the weak acid environment, potentially due to the disruption of crosslinked structures or chemical bonds under acidic conditions (Fig. 2E). To investigate the release profile of MitoQ from the hydrogels, FITC-labelled MitoQ was loaded into 12.5%/12.5% hydrogels, and subsequent *in vitro* release studies were conducted (Fig. 2F). The *in vitro* release profile of MitoQ was determined by measuring the UV absorbance at 490 nm of a 1 mL sample solution extracted from the release medium at specific time intervals. The experimental results demonstrated that about 90% or more of MitoQ was released from the hydrogel within 8 days at pH 6.0, which was higher than that of the pH 7.5 (Fig. 2F). These findings provide concurrent validation of the hydrogels' capability to maintain structural integrity and release MitoQ during the early stages of MI, thereby ensuring their therapeutic efficacy.

$NH_2$-γ-PGA-DA/4-arm-PEG-SG hydrogels exhibit notable tissue adhesion properties attributed to their abundant phenolic hydroxyl and amino groups. Tissue adhesion experiments were conducted to explore the adhesive properties of this hydrogel. The $NH_2$-γ-PGA-DA/4-arm-PEG-SG hydrogel exhibited robust adhesion to vital tissues, including the heart, liver, spleen, lung, and kidney. This adhesion primarily resulted from the formation of various non-covalent and covalent bonds between phenolic hydroxyls in the gel and different nucleophilic reagents, such as amines, thiols, and carboxyl groups (Fig. 2G). Moreover, we evaluated the *in vitro* tissue adhesion of $NH_2$-γ-PGA-DA/4-arm-PEG-SG hydrogels using freshly obtained porcine skin tissue. Specifically, the adhesion strength of the 12.5 wt%/12.5 wt% hydrogels measured 12.0 ± 0.6 kPa, surpassing the 10.2 ± 0.5 kPa adhesion strength of the 15 wt%/15 wt% hydrogels (Fig. 2H). The adhesion of hydrogels is influenced by their surface properties and interactions with other substances. As the strength of a hydrogel increases, its surface tends to become smoother and harder, reducing contact area and ability to interact with other substances. Moreover, higher strength in hydrogels may result in increased surface tension, making it harder for them to adhere to other materials. Hydrogels with a 15 wt% composition exhibit higher mechanical strength and less contact area than those with a 12 wt% composition, resulting in weakened adhesion properties. This does not imply inferiority, but rather highlights the delicate balance between mechanical properties and adhesion. In summary, hydrogels composed of 12.5 wt% $NH_2$-γ-PGA-DA/12.5 wt% 4-arm-PEG-SG exhibit noteworthy adhesion properties, suitable gelation time, and mechanical characteristics, positioning them as potential candidates for hydrogel patches.

### 3.3 *In vitro* effects of the MitoQ/hydrogels on ROS scavenging

The biocompatibility of hydrogels plays a crucial role in cell growth, differentiation, and migration. We assessed the impact of each hydrogel component on CM activity by employing the CCK-8 assay. The experimental results indicated that the effects of different hydrogel extracts on CM activity did not exhibit statistical significance (Fig. 3A). In addition, we utilized a live/dead cell staining kit to assess CM viability during cell culture. By combining calcineurin AM and PI staining, we observed minimal presence of dead cells within the hydrogel, and the CMs exhibited sustained viability even after 7 days of culture, indicating the favorable cytocompatibility of the hydrogel (Fig. 3B).

Acute ischemia-reperfusion (I/RI) injury following MI primarily occurs due to mitochondrial dysfunction and the generation of ROS, which serves as the main trigger for apoptosis.[27] Subsequently, the release of numerous intracellular molecules prompts the recruitment of inflammatory cells into the infarcted region, resulting in the expression of pro-inflammatory cytokines and further exacerbating the inflammatory process.[27,28] To prevent apoptosis and the subsequent inflammatory cascade following infarction, early intervention to inhibit CM

 

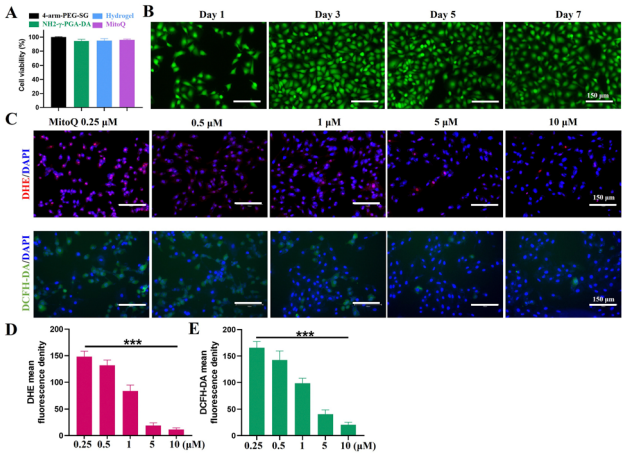


Fig. 3 Effect of the MitoQ/hydrogels on oxidative damage in CMs. (A) Effect of different components on CM activity. (B) Live-dead staining of CMs incubated on hydrogels for one week. (C) Representative fluorescence images of DHE and DCFH-DA in $H_2O_2$ induced cells treated with different concentrations of MitoQ. (D) and (E) Fluorescence semi-quantitative analysis of DHE and DCFH-DA. ($n$ = 3, *$p$ < 0.05, **$p$ < 0.01, and ***$p$ < 0.001).

mitochondrial damage and mitigate ROS production is imperative. MitoQ, an antioxidant specifically targeting mitochondria, retards oxidative stress-induced damage to mitochondria and enhances cellular energy, thereby promoting organ function improvement.[29] Previous studies have demonstrated the efficacy of MitoQ in alleviating mitochondrial damage primarily through the regulation of redox-related non-coding RNAs associated with cardiac remodeling.[30] The effectiveness of MitoQ concentration is influenced by both low and excessive levels, as they may result in ineffectiveness or adverse effects respectively. By amalgamating the instructions for MitoQ usage and previous literature reports, we ultimately selected a concentration gradient ranging from 0.25 μM to 10 μM for *in vitro* experiments.[31–33] To examine the impact of MitoQ on the modulation of intracellular ROS levels in CMs, we employed an $H_2O_2$-induced oxidative stress injury model in CMs. Dihydroethidium (DHE) and 2,7-dichlorodihydrofluorescein diacetate (DCFH-DA) staining were employed to measure the intracellular levels of superoxide anions and hydroxyl radicals. After a 12-hour $H_2O_2$ treatment, the control CMs displayed strong DHE red fluorescence and DCFH-DA green fluorescence, indicative of heightened intracellular ROS levels (Fig. 3C–E). Upon the addition of MitoQ, the intracellular fluorescence intensity of DHE and DCFH-DA decreased. The fluorescence intensity of DHE and DCFH-DA decreased as the concentration of MitoQ increased, with the desired antioxidant effect observed at 5 μM. While 10 μM MitoQ demonstrated significant antioxidant effects, a higher dosage was necessary. Furthermore, other studies have indicated that high doses of MitoQ resulted in a slight 5% decrease in the viability of H9C2 cells.[34] Therefore, we selected 5 μM MitoQ for our study in the subsequent experiments.

### 3.4 Effect of the MitoQ/hydrogel on CM mitochondria

Myocardial ischemia and hypoxia directly impact the structure and function of CM mitochondria. To examine the impact of MitoQ/hydrogel on oxidative damage in CMs, we induced CM damage using $H_2O_2$ and observed the structural changes of CM mitochondria in various treatment groups using bioTEM. Mitochondrial damage was characterized by a transition from a reticular to a fragmented structure and alterations in outer membrane permeability. In contrast to the severe mitochondrial damage and cell membrane rupture induced by $H_2O_2$, the MitoQ-containing group and the MitoQ/hydrogel group effectively mitigated structural mitochondrial damage, leading to improved integrity of the mitochondrial cristae and cell membranes (Fig. 4A). Additionally, we utilized the JC-1 kit to assess the mitochondrial membrane potential of CMs treated with various hydrogel samples. The $H_2O_2$ group exhibited significantly higher green fluorescence values compared to the control group, suggesting compromised mitochondrial function. Likewise, CMs treated with MitoQ/hydrogel exhibited markedly reduced fluorescence intensity in mitochondrial membrane potential, providing strong evidence for the antioxidant effect of MitoQ/hydrogel (Fig. 4B and C). In conclusion, MitoQ/hydrogel can suppress ROS production by enhancing mitochondrial membrane potential and structure, consequently enhancing CM activity.

### 3.5 Effects of the MitoQ/hydrogel on cardiac structure in rats with MI

Although high-performance myocardial patches may offer superior therapeutic benefits for MI, they are not suitable for use as injectable hydrogels in intramyocardial injection therapy simultaneously. The main objective of the study was to compare the therapeutic efficacy of two strategies with identical formulations and analyze various reasons for differences observed. The implications of these reasons provide valuable insights for future studies. Additionally, mechanically weak myocardial patches have advantages, such as serving as a gentle

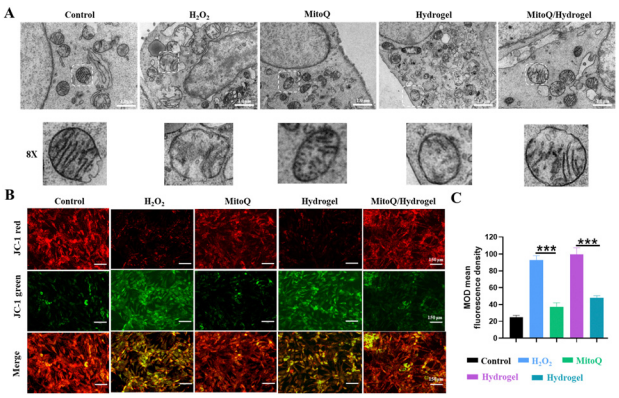


Fig. 4 Effects of the MitoQ/hydrogel on mitochondrial structure and function. (A) Bio-TEM images of CM mitochondria from different treatment groups (Scale bars: 1 μm). (B) Representative JC-1 fluorescence images of CM mitochondrial membrane potential in different treatment groups. Green fluorescence indicates a compromised mitochondrial membrane potential, signifying the early onset of apoptosis, whereas red fluorescence indicates an intact mitochondrial membrane potential and healthy cells. (C) Quantitative analysis of JC-1 fluorescence intensity values. ($n$ = 3, *$p$ < 0.05, **$p$ < 0.01, and ***$p$ < 0.001).

scaffold with large aperture channels that facilitate cell proliferation and migration, thus aiding in tissue repair and regeneration. The low mechanical strength of the hydrogel reduces surgical trauma and invasiveness compared to high-strength materials, making the procedure less complex and risky due to its softness, which allows for easier injection or adhesion to the infarcted myocardial area. To compare the therapeutic effects of hydrogel intracardiac injection and hydrogel myocardial patch, we identified four experimental groups in this study: the normal group, saline group, MitoQ/patch group, and MitoQ/hydrogel intracardiac injection group. Given the *in situ* release of MitoQ from the hydrogel, we utilized the same concentration (*i.e.*, 5 μM of MitoQ loaded in 100 mL hydrogel) for our *in vivo* experiments. After subjecting rats to MI for 3 days, we extracted their hearts for H&E and Masson staining. The results revealed that both the MitoQ/hydrogel myocardial patch and intramyocardial injection treatments did not induce any notable adverse effects on myocardial tissues, such as significant inflammation (Fig. 5A and B). To verify the impact of MitoQ/hydrogel on ROS clearance during the early stage of MI, we assessed the superoxide anion level in the infarct area after 5 days of treatment using DHE staining. The results demonstrated that the saline-injected group exhibited a strong DHE signal, while the DHE signal in the MitoQ/hydrogel-injected group was significantly attenuated, suggesting the effective elimination of ROS accumulation in the infarct region of the myocardium by MitoQ (Fig. 5C). Notably, the intramyocardial injection of MitoQ/hydrogel group exhibited the most substantial reduction in the DHE signal, highlighting the significant inhibition of ROS generation during the early stage of myocardial ischemia by intramyocardial injection of MitoQ/hydrogel. Furthermore, we evaluated the extent of mitochondrial damage in the myocardium to further assess the therapeutic effects of the released MitoQ concentration. By using transmission electron microscopy, we observed a significant improvement in mitochondrial cristae damage, indicating the effective elimination of ROS at this concentration (Fig. 5D). In summary, these findings indicate that while the concentration of MitoQ loaded in the hydrogel may not be ideal, it is sufficient for effective scavenging of ROS.

On day 5 of treatment, apoptosis was detected in all groups using TUNEL staining. The TUNEL staining results confirmed a significant increase in the number of surviving CMs in the infarcted region of the myocardium after treatment with MitoQ/injection, surpassing all other groups (Fig. 5E). However, the MitoQ/patch group did not exhibit a significant therapeutic advantage, potentially due to the inconsistency between the drug release cycle in the patch and intramyocardial injection. The inhibition of CM apoptosis coincided with reduced inflammation and an increased predominance of M2 macrophages, facilitating angiogenesis in the infarcted area. CD31 immunofluorescence results revealed a significantly greater vessel density in the infarcted area of the MitoQ/injection group compared to the other groups, further confirming the potential therapeutic efficacy of MitoQ/injection in enhancing CM activity (Fig. 5F).

The experimental timeline of rats with MI is illustrated in Fig. 6A. Both the MitoQ/hydrogel myocardium administration group and the patch group exhibited inhibited infarct enlargement and reduced fibrotic area compared to the saline group (Fig. 6B–E). Importantly, the MitoQ/hydrogel myocardial administration group demonstrated more substantial improvement in the apical, mid, and upper segments of the heart, as well as an increase in myocardial wall thickness, in comparison to the MitoQ/hydrogel patch group. We examined the primary reasons for the disparity between these two treatment modalities: (i) the cardiac patch exhibits weaker mechanical properties and provides less robust mechanical support on the myocardial surface, consequently inadequately mitigating myocardial loading and inhibiting myocardial remodeling. (ii) The distribution of the hydrogel throughout the entire area of infarcted myocardial tissue *via* the injection modality results in broader coverage and hence homogeneous therapeutic effects. Conversely, the cardiac patch is predominantly confined to the patch-covered area, which represents a smaller coverage and thus only generates an effective therapeutic effect in the localized region. (iii) Given the densely packed structure of the myocardial surface, it may be challenging for the drug in the patch to penetrate the lesion. To enhance the therapeutic effect, efficient delivery of the drug into the myocardium using microneedles is necessary, thereby producing a more substantial and uniform therapeutic effect.

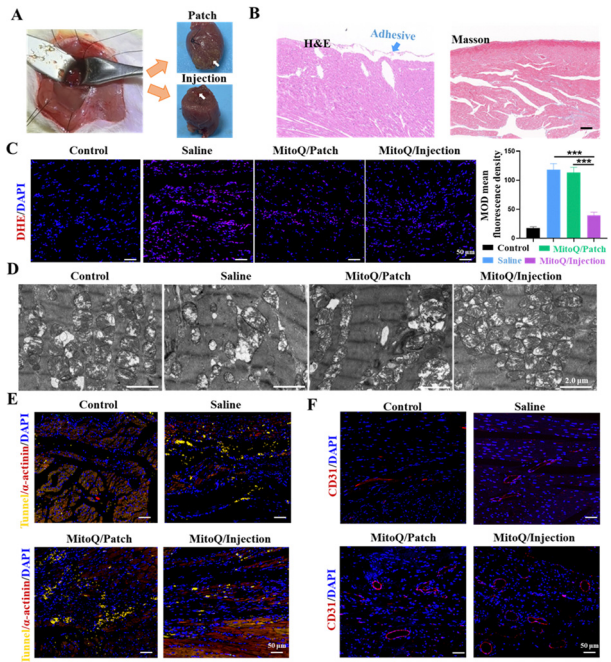


Fig. 5 Effect of MitoQ/hydrogel on ROS and apoptosis in the MI region. (A) Photographs of isolated hearts after 3 days of hydrogel as a myocardial patch and intramyocardial injection for MI treatment. (B) H&E and Masson staining of isolated hearts 3 days after treatment. (C) DHE staining and DHE fluorescence quantification of infarct sites after 5 days of treatment in different treatment groups. (D) Effect of MitoQ/hydrogel on the mitochondria of CMs in the MI region. (scale bars: 2 μm). (E) Representative immunofluorescence images of CMs with Tunnel, α-actinin, and DAPI staining at the infarct site. (F) Representative immunofluorescence fluorescent images of CD31 and DAPI staining at the infarct site. ($n$ = 3, $^{*}p < 0.05$, $^{**}p < 0.01$, and $^{***}p < 0.001$).

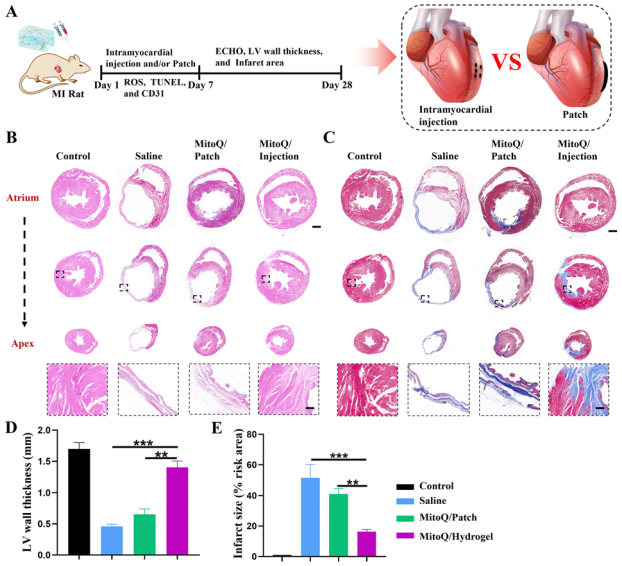


Fig. 6 Effect of the MitoQ/hydrogel on myocardial structure in infarcted rats. (A) Experimental timeline of hydrogel-treated infarcted rats. (B) and (C) H&E and Masson staining of MI in different treatment groups. Scale bars: 1 mm; enlarged images: 100 μm. (D) Quantification of LV myocardial wall thickness in different treatment groups. (E) Quantification of myocardial fibrosis area in different treatment groups. ($n$ = 3, *$p$ < 0.05, **$p$ < 0.01, and ***$p$ < 0.001).

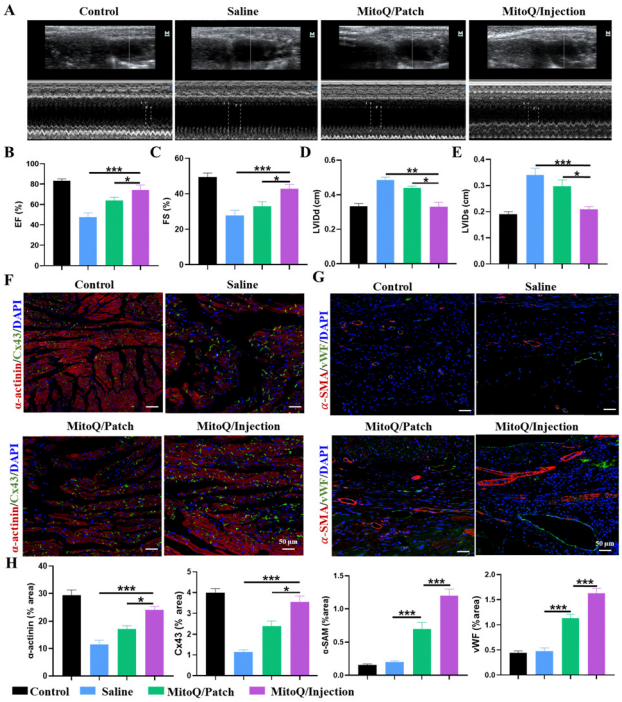


Fig. 7 Effects of the MitoQ/hydrogel on cardiac function in rats with MI. (A) ECHO of SD rats in different treatment groups after treatment for 28 days. (B)–(E) EF, FS, LVIDd, and LVIDs were obtained by ECHO. (F) Fluorescence semiquantitative analysis of Cx43, α-actinin, α-SMA, and vWF levels. (G) Representative immunofluorescence images of α-actinin and Cx43 from different treatment groups. (H) Fluorescence quantification of α-actinin, Cx43, α-SMA, and vWF. (Scale bars: 100 μm, $n$ = 3, *$p$ < 0.05, **$p$ < 0.01, and ***$p$ < 0.001).

### 3.6 Effects of the MitoQ/hydrogel on cardiac function in rats with MI

Echocardiography (ECHO) was performed after 28 days of treatment to evaluate cardiac function in all groups (Fig. 7A–E). The results indicated that the saline and blank hydrogel groups displayed characteristic manifestations of MI, including a significant reduction in cardiac LVEF and LVFS, and a significant increase in LVESV and LVEDV. In contrast, both the MitoQ/hydrogel intracardiac delivery group and the MitoQ/hydrogel patch group exhibited elevated LVEF and LVFS, along with reduced LVESV and LVEDV, suggesting enhanced pump function and ventricular filling. Particularly, the enhancement in LVEF, LVFS, LVESV, and LVEDV was more prominent in the MitoQ/hydrogel intracardiac administration group compared to the hydrogel patch group.

Angiogenesis is essential for myocardial repair or regeneration following MI as it reinstates oxygen and nutrient delivery to the infarcted region and enhances the survival of CMs. After a 28-day treatment period, the expression of angiogenic proteins and extracellular matrix gap junction proteins was assessed in the infarcted area of all groups. Immunofluorescence staining, utilizing the vascular-specific markers α-smooth muscle actin (α-SMA) and von Willebrand factor (vWF), revealed a notable augmentation in microvessel density in both the MitoQ/hydrogel intracardiac administration group and the patch group. Quantitative analyses demonstrated a significantly greater microvessel density in the MitoQ/hydrogel intracardiac administration group in comparison to the other groups, surpassing the hydrogel patch treatment group (Fig. 7F and H). Immunofluorescence staining was utilized to evaluate the expression of cytoskeletal structure (α-actinin) and gap junction protein (Cx43) in the infarcted area (Fig. 7G and H). The MitoQ/hydrogel-injected group exhibited better preservation of α-actinin-labeled myocardial transverse structures compared to the MitoQ/patch-treated group, along with the highest expression level of Cx43. Collectively, these findings indicate that both intracardiac injection of MitoQ/hydrogel and MitoQ/hydrogel patch can enhance the structure and function of MI; however, intracardiac injection of MitoQ/hydrogel may exhibit superior therapeutic effects.

Although high-performance myocardial patches may offer superior therapeutic benefits for MI, they are not suitable for use as injectable hydrogels in intramyocardial injection therapy simultaneously. To ensure consistency between the two therapeutic formulations, we opted for a mechanically weak myocardial patch in this study. Although this myocardial patch with weak mechanical strength may not be fully representative, this study elucidates the variations in MI treatment utilizing the same hydrogel formulation, providing reference into the underlying causes.

## 4. Discussion

Both intracardiac injectable hydrogels and hydrogel heart patches promote myocardial regeneration and repair by providing

mechanical support and creating a suitable biological environment. They vary in their treatment modalities and application locations, with intramyocardial injectable hydrogels primarily exerting their therapeutic effects through direct injection into myocardial tissue, while hydrogel cardiac patches are affixed to the myocardial surface. The specific therapeutic effect and mechanism may be influenced by several factors, including the mechanical properties of the hydrogel, the therapeutic range, and the severity of the condition. In this study, we utilized these two modalities to compare the differences following the treatment of MI. The results indicate that both treatment modalities effectively address MI when analyzed at the apex, middle, and base of the heart tissue, except that the myocardial injection modality yields a more uniform effect. We examined the primary reasons for the disparity between these two treatment modalities: (i) the cardiac patch exhibits weaker mechanical properties and provides less robust mechanical support on the myocardial surface, consequently inadequately mitigating myocardial loading and inhibiting myocardial remodeling. (ii) The distribution of the hydrogel throughout the entire area of infarcted myocardial tissue *via* the injection modality results in broader coverage and hence homogeneous therapeutic effects. Conversely, the cardiac patch is predominantly confined to the patch-covered area, which represents a smaller coverage and thus only generates an effective therapeutic effect in the localized region. (iii) Given the densely packed structure of the myocardial surface, it may be challenging for the drug in the patch to penetrate the lesion. To enhance the therapeutic effect, efficient delivery of the drug into the myocardium using microneedles is necessary, thereby producing a more substantial and uniform therapeutic effect.

In conclusion, addressing the problem of mitochondrial damage in a significant number of CMs following MI, we have developed a MitoQ-loaded $NH_2$-γ-PGA-DA/4-arm-PEG-SG hydrogel system. The optimized hydrogel formulation not only possessed the necessary adhesion properties for the myocardial surface but also facilitated deep myocardial injection. *In vitro* studies indicated that the controlled release of MitoQ from the hydrogel system enhanced mitochondrial function and augmented cellular activity in cardiomyocytes. *In vivo* results demonstrated that both intramyocardial and extramyocardial administration of the hydrogel in rats after MI suppressed mitochondrial damage, scavenged ROS, enhanced cardiomyocyte activity, and facilitated improved cardiac function. Importantly, Intramyocardial injection of the hydrogel results in a more uniform therapeutic effect, while the myocardial patch can target specific infarct sites. This simply prepared prepared MitoQ/hydrogel system holds immense potential for MI treatment and offers substantial clinical translational benefits.

## Author contributions

Ying Tan: conceptualization, methodology, formal analysis, writing – original draft, writing – review & editing. Yali Nie and ZhengWen Lei: animal model construction, methodology, and formal analysis. Zhi Zheng: writing – original draft, writing-review & editing.

## Conflicts of interest

There are no conflicts to declare.

## Acknowledgements

This work was supported by National Natural Science Foundation of China (82304429), Key R & D Program of Hunan Province (2021SK2036), Post-doctoral funding from the University of South China (220XQD106), Natural Science Foundation of Hunan Province (2023JJ40570), Science and Technology Innovation Plan Project of Hunan Province (2020sk51824), and Natural Science Foundation of Hunan Province (2023JJ50152).

## Notes and references

1 G. H. L. Tang, R. Estevez-Loureiro, Y. Yu, J. B. Prillinger, S. Zaid and M. A. Psotka, *J. Am. Heart Assoc.*, 2021, **10**, e019882.
2 D. M. Christensen, J. E. Strange, M. El-Chouli, A. C. Falkentoft, M. Malmborg, N. Nouhravesh, G. Gislason, M. Schou, C. Torp-Pedersen and T. S. G. Sehested, *J. Am. Coll. Cardiol.*, 2023, **82**, 971–981.
3 T. J. Siddiqi, A. M. Khan Minhas, S. J. Greene, H. G. C. Van Spall, S. S. Khan, A. Pandey, R. J. Mentz, G. C. Fonarow, J. Butler and M. S. Khan, *JACC. Heart Fail.*, 2022, **10**, 851–859.
4 X. Yuan and T. Braun, *Circ. Res.*, 2017, **121**, 293–309.
5 M. Ponnusamy, F. Liu, Y. H. Zhang, R. B. Li, M. Zhai, F. Liu, L. Y. Zhou, C. Y. Liu, K. W. Yan, Y. H. Dong, M. Wang, L. L. Qian, C. Shan, S. Xu, Q. Wang, Y. H. Zhang, P. F. Li, J. Zhang and K. Wang, *Circulation*, 2019, **139**, 2668–2684.
6 T. M. A. Mohamed, Y. S. Ang, E. Radzinsky, P. Zhou, Y. Huang, A. Elfenbein, A. Foley, S. Magnitsky and D. Srivastava, *Cell*, 2018, **173**, 104–116e112.
7 W. Chen, C. Wang, W. Liu, B. Zhao, Z. Zeng, F. Long, C. Wang, S. Li, N. Lin and J. Zhou, *Adv. Mater.*, 2023, **35**, e2209041.
8 P. Li, J. Hu, J. Wang, J. Zhang, L. Wang and C. Zhang, *Bioengineering*, 2023, **10**, 165.
9 Y. Zhu, X. Yang, J. Zhou, L. Chen, P. Zuo, L. Chen, L. Jiang, T. Li, D. Wang, Y. Xu, Q. Li and Y. Yan, *Oxid. Med. Cell. Longevity*, 2022, **2022**, 3182931.
10 A. C. Cardoso, N. T. Lam, J. J. Savla, Y. Nakada, A. H. M. Pereira, A. Elnwasany, I. Menendez-Montes, E. L. Ensley, U. B. Petric, G. Sharma, A. D. Sherry, C. R. Malloy, C. Khemtong, M. T. Kinter, W. L. W. Tan, C. G. Anene-Nzelu, R. S. Foo, N. U. N. Nguyen, S. Li, M. S. Ahmed, W. M. Elhelaly, S. Abdisalaam, A. Asaithamby, C. Xing, M. Kanchwala, G. Vale, K. M. Eckert, M. A. Mitsche, J. G. McDonald, J. A. Hill, L. Huang, P. W. Shaul, L. I. Szweda and H. A. Sadek, *Nat. Metab.*, 2020, **2**, 167–178.

 

11 D. Boulghobra, P. E. Grillet, M. Laguerre, M. Tenon, J. Fauconnier, P. Fança-Berthon, C. Reboul and O. Cazorla, *Redox Biol.*, 2020, **34**, 101554.
12 B. N. Puente, W. Kimura, S. A. Muralidhar, J. Moon, J. F. Amatruda, K. L. Phelps, D. Grinsfelder, B. A. Rothermel, R. Chen, J. A. Garcia, C. X. Santos, S. Thet, E. Mori, M. T. Kinter, P. M. Rindler, S. Zacchigna, S. Mukherjee, D. J. Chen, A. I. Mahmoud, M. Giacca, P. S. Rabinovitch, A. Aroumougame, A. M. Shah, L. I. Szweda and H. A. Sadek, *Cell*, 2014, **157**, 565–579.
13 F. Wang and J. Guan, *Adv. Drug Delivery Rev.*, 2010, **62**, 784–797.
14 Z. Zheng, Y. Tan, Y. Li, Y. Liu, G. Yi, C. Y. Yu and H. Wei, *J. Controlled Release*, 2021, **335**, 216–236.
15 Z. Zheng, C. Lei, H. Liu, M. Jiang, Z. Zhou, Y. Zhao, C. Y. Yu and H. Wei, *Adv. Healthcare Mater.*, 2022, **11**, e2200990.
16 P. Lesizza, G. Prosdocimo, V. Martinelli, G. Sinagra, S. Zacchigna and M. Giacca, *Circ. Res.*, 2017, **120**, 1298–1304.
17 T. Yoshizumi, Y. Zhu, H. Jiang, A. D'Amore, H. Sakaguchi, J. Tchao, K. Tobita and W. R. Wagner, *Biomaterials*, 2016, **83**, 182–193.
18 Y. Wang, Z. Fan, Q. Li, J. Lu, X. Wang, J. Zhang and Z. Wu, *J. Mater. Chem. B*, 2023, **11**, 4980–4990.
19 W. Li, P. Chen, Y. Pan, L. Lu, X. Ning, J. Liu, J. Wei, M. Chen, P. Zhao and C. Ou, *Adv. Sci.*, 2022, **9**, e2204509.
20 M. Domenech, L. Polo-Corrales, J. E. Ramirez-Vick and D. O. Freytes, *Tissue Eng., Part B*, 2016, **22**, 438–458.
21 S. Shen, J. Zhang, Y. Han, C. Pu, Q. Duan, J. Huang, B. Yan, X. You, R. Lin, X. Shen, X. Qiu and H. Hou, *Adv. Healthcare Mater.*, 2023, **12**, e2301990.
22 Z. Zheng, Z. Guo, F. Zhong, B. Wang, L. Liu, W. Ma, C. Y. Yu and H. Wei, *J. Controlled Release*, 2022, **347**, 127–142.
23 C. Shuai, W. Yang, P. Feng, S. Peng and H. Pan, *Bioact. Mater.*, 2021, **6**, 490–502.
24 M. Cao, J. Feng, S. Sirisansaneeyakul, C. Song and Y. Chisti, *Biotechnol. Adv.*, 2018, **36**, 1424–1433.
25 N. Frey, A. Linke, T. Süselbeck, J. Müller-Ehmsen, P. Vermeersch, D. Schoors, M. Rosenberg, F. Bea, S. Tuvia and J. Leor, *Circ.: Cardiovasc. Interventions*, 2014, **7**, 806–812.
26 C. Fan, J. Shi, Y. Zhuang, L. Zhang, L. Huang, W. Yang, B. Chen, Y. Chen, Z. Xiao, H. Shen, Y. Zhao and J. Dai, *Adv. Mater.*, 2019, **31**, e1902900.
27 C. J. A. Ramachandra, S. Hernandez-Resendiz, G. E. Crespo-Avilan, Y. H. Lin and D. J. Hausenloy, *EBioMedicine*, 2020, **57**, 102884.
28 N. Abbas, F. Perbellini and T. Thum, *Basic Res. Cardiol.*, 2020, **115**, 52.
29 R. Ning, Y. Li, Z. Du, T. Li, Q. Sun, L. Lin, Q. Xu, J. Duan and Z. Sun, *Redox Biol.*, 2021, **46**, 102113.
30 F. Rostamzadeh, H. Najafipour, S. Aminizadeh and E. Jafari, *Biomed. Pharmacother.*, 2024, **170**, 116020.
31 D. Graham, N. N. Huynh, C. A. Hamilton, E. Beattie, R. A. Smith, H. M. Cochemé, M. P. Murphy and A. F. Dominiczak, *Hypertension*, 2009, **54**, 322–328.
32 K. Y. Goh, L. He, J. Song, M. Jinno, A. J. Rogers, P. Sethu, G. V. Halade, N. S. Rajasekaran, X. Liu, S. D. Prabhu, V. Darley-Usmar, A. R. Wende and L. Zhou, *Redox Biol.*, 2019, **21**, 101100.
33 A. J. Dare, A. Logan, T. A. Prime, S. Rogatti, M. Goddard, E. M. Bolton, J. A. Bradley, G. J. Pettigrew, M. P. Murphy and K. Saeb-Parsy, *J. Heart Lung Transplant.*, 2015, **34**, 1471–1480.
34 V. Peugnet, M. Chwastyniak, P. Mulder, S. Lancel, L. Bultot, N. Fourny, E. Renguet, H. Bugger, O. Beseme, A. Loyens, W. Heyse, V. Richard, P. Amouyel, L. Bertrand, F. Pinet and E. Dubois-Deruy, *Antioxidants*, 2022, **11**, 723.